2024 IEEE/RSJ International Conference on Intelligent Robots and Systems (IROS)
October 14-18, 2024. Abu Dhabi, UAE

OBHMR: Robust Partial-to-full Generalized Point Set Registration with Overlap-guided Bidirectional Hybrid Mixture Model

Xinzhe Du†, Zhengyan Zhang†, Ang Zhang, Rui Song, Yibin Li, Max Q.-H. Meng, *IEEE Fellow*, Zhe Min⋆

***Abstract*— In this paper, we introduce a novel overlap-based bidirectional point set registration approach, i.e., Overlap-guided Bidirectional Hybrid Mixture Registration (OBHMR), which incorporates geometric information (i.e., normal vectors) in both the correspondence and transformation stages and formulates the optimization objective of registration in a bidirectional manner. More importantly, to address the issue of partial-to-full registration, OBHMR utilises the predicted point-wise overlap score using networks to formulate the overlap-guided Hybrid Mixture Model consisting of the Gaussian Mixture Model (GMM) and Fisher Mixture Model (FMM). OBHMR contains four components: (1) the overlap-guided correspondence network that estimates the correspondence probabilities and calculates the point-wise overlap score; (2) the learning posterior module that estimates the overlap-guided HMM parameters; (3) the transformation module that computes the rigid transformation by formulating the optimisation objective in a bidirectional registration way, given correspondences and overlap-guided HMM parameters. Experiments using 1457 human femur and 1301 human hip models demonstrate significant improvements in partial-to-full registration performance ($p < 0.01$) under different overlapping ratios, compared to state-of-the-art registration approaches. Furthermore, individual contributions of three modules (i.e., additional normal vectors, overlap score estimation module and the bidirectional mechanism) in OBHMR have been validated in ablation studies. The results demonstrate OBHMR's capability of tackling the challenging partial-to-full registration problems in computer-assisted orthopedic surgery. The codes are available at https://github.com/Dxinz/DeepOBHMR.**

I. INTRODUCTION

Point set registration is a fundamental problem that affects the interventional accuracy in medical robots system [1] or computer-assisted orthopedic surgery (CAOS) [2]. In CAOS, surgical procedures are performed by either the surgeon or a robotic system in the patient frame. Rigid registration is thus needed to align pre-operative and intra-operative spaces together, enabling the surgeon to refer to the correctly transformed pre-operative model (and the surgical plan) during surgery, on the computer monitor or with augmented-reality glasses [3]. Generally speaking, the surgical plan includes the determination of entry points and surgical paths, and the identification (e.g., segmentation) of critical structures to avoid. In CAOS, point sets in preoperative and intraoperative spaces are derived from medical images (i.e., CT and MRI) and measurements taken using an optically tracked stylus, respectively. On one hand, both point sets in two spaces could contain noise and outliers [4]. On the other hand, intraoperative points are partial subsets of the full preoperative model, which makes it difficult to seek the correct point correspondences [5]. Therefore, achieving robust (w.r.t. noise and outliers) partial-to-full registrations in CAOS is a challenging task.

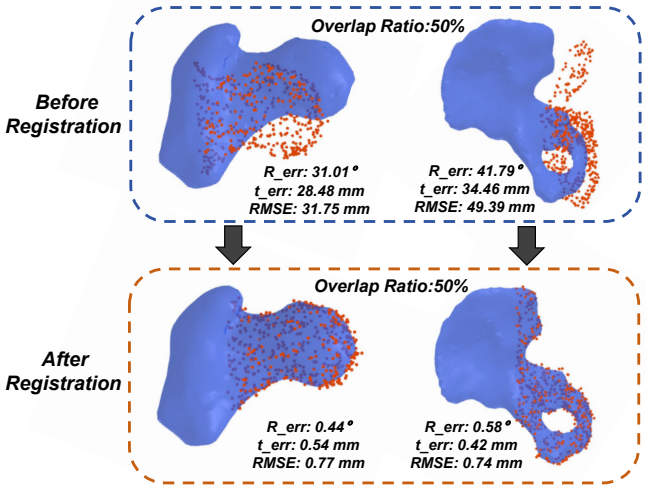

Fig. 1. The figure above shows the registration results of our method with a 50% overlap ratio and noise, between the partial intra-operative point set and the full pre-operative point set. The partial and full point sets are shown in red points and blue surface respectively.

Motivations. In this paper, we combine the hybrid registration framework, the overlap prediction and the bidirectional mechanism to solve the partial-to-full registration problem. The motivations of this paper are two-fold. *On one hand*, although hybrid registration methods (e.g., DeepGMR [6] and UGMM [7]) achieve great robustness to noise, they typically require two point sets to share the same Gaussian Mixture Model (GMM) parameters. However, in

†Equal Contributions, ⋆Corresponding Author.

This work was supported in part by the National Natural Science Foundation of China under Grant 62303275, National Natural Science Fund for Excellent Young Scientists Fund Program (Overseas) under Grant 22IAA01849, and Jinan Science and Technology Bureau under Grant 202333011.

Xinzhe Du, Rui Song, Yibin Li and Zhe Min are with the School of Control Science and Engineering, Shandong University, China. Zhe Min is also with the Wellcome/EPSRC Centre for Interventional and Surgical Sciences, University College London, London, UK (minzhe@sdu.edu.cn).

Zhengyan Zhang is with the Department of Aeronautical and Aviation Engineering, The Hong Kong Polytechnic University.

Ang Zhang is with Yuanhua Robotics, Perception and AI Technologies Ltd, Shenzhen, China.

Max Q.-H. Meng is with the Department of Electronic and Electrical Engineering of the Southern University of Science and Technology, Shenzhen, China.

CAOS, the intraoperative point set covers a partial region of the preoperative full model, which indicates the GMMs estimated from the two point sets are different. To solve the partial-to-full registration, the overlap prediction module is added to the hybrid mixture model (HMM) registration framework. *On the other hand*, most probabilistic registration methods (e.g., CPD [8] and BCPD [9]) assume that one point set is perfect while the other contains noise and outliers. However, noise and outliers exist in both point sets in real-world scenarios. Thus, the bidirectional registration process is carefully formulated to consider noise and outliers in both point sets while additional normal vectors are also leveraged to enhance the robustness to noise.

Contributions. In this paper, we present the Overlap-guided Bi-directional Generalised Point Set Registration (OBHMR) method. The contributions are summarised as follows. First, an overlap prediction module is added to the registration framework to estimate the parameters (i.e., point-wise overlap score) utilised in the overlap-guided HMM, consisting of GMMs for position vectors and FMMs for normal vectors. The overlap-guided HMM registration problem is then correspondingly formulated. Second, the bi-directional registration mechanism is utilised in OBHMR, where the optimization objective consists of the KL divergence between the transformed source point set and latent target HMM, and that between the transformed target point set and latent source HMM. Finally, OBHMR is evaluated against state-of-the-art registration approach on the medical point set dataset (i.e., MedShapeNet) consisting of 1457 femur and 1301 hip shapes, which validate OBHMR's strong capability to handle partial-to-full registration under different overlap ratios and shapes.

Organization. The remainder of this paper is organized as follows. Sect. II introduces relevant rigid point set registration methods in the literature. Sect. III describes the partial generalized rigid point set registration problem. Sect. IV formally formulates overlap-based hybrid mixture model and defines the two-step optimization problem. Sect. V describes the proposed OBHMR approach in detailS. Sect. VI presents experiments and results. Sect. VII concludes the paper.

II. Related Work

We review the relevant rigid point set registration methods, which are categorised into conventional, learning-based and hybrid registration approaches.

A. Conventional Registration Methods

Conventional registration methods utilise optimization strategies to estimate the rigid transformation. Iterative Closest Point (ICP) [10] iteratively updates point correspondences and estimates the rigid transformation matrix, which is susceptible to noise and outliers. Coherent Point Drift [8] treats points in one point set as centroids of one GMM and the other point set being sampled by the transformed GMM using the desired transformation, and formulates the regsitration as a probability density estimation problem. BCPD [9] adapts CPD within a Bayesian framework, thereby ensuring theoretical convergence. Both in CPD [8] and BCPD [9], one point set is considered to be perfect while the other contains noise and outliers.

B. Hybrid Registration Methods

The hybrid registration methods involve three steps: learning points feature with neural networks, casting point sets as probability density functions (i.e., hybrid models), and then minimising the distance of two hybrid models. DeepGMR [6] is a milestone in this line of research, which comprises two sequential components: (1) the correspondence network that estimates point-to-distribution correspondence probabilities, (2) the parameter-free computation blocks that calculate GMM parameters and the rigid transformation respectively. With the assumption that two point sets are sampled from a unified GMM, UGMM [7] first learns point-to-distribution correspondences and then estimates the unified GMM parameters, afterwards computes rigid transformations between point sets and the unified GMM. It is noticed that only positional information is utilised in hybrid registration methods (e.g., DeepGMR [6] and UGMM [7]).

C. Learning-based Registration Methods

FMR [11] solves the registration problem by minimizing the projection error within the feature space in a semi-supervised manner. PointNetLK++ [12] overcomes the limitations of PointNetLK, by analytically computing the Jacobian of PointNet features concerning the exponential map *twist* parameters. For partial-to-full registration, some learning-based methods use neural networks to predict the overlap region in point sets. Predator[13], designed for registering point sets with low overlap, is composed of three key modules: an encoder that extracts superpoints and associated features, an overlap-attention module that captures co-contextual information between the two point sets, and a decoder that predicts per-point feature, overlap score, and matchability score. In RegTr [14], the KPConv backbone [15] is employed to extract downsampled superpoints along with their features, and then the transformer cross-encoder together with output layer are then utilised to predict the transformed superpoints and overlap scores, with which the optimal rigid transformation is computed using the weighted Kabsch-Umeyama algorithm [16]. On top of DeepGMR, OGMM [17] develops a clustering-based transformer module that predicts the point-wise overlap score in two point sets, and then establishes the overlap-guided GMM to solve the partial point set registration problem.

III. The Partial Generalized Rigid Point Set Registration with Overlap

We first formally formulate the point set registration problem, where both positional and normal information is leveraged. One source generalised point is defined as $\mathbf{d}_n^p = [\mathbf{p}_n^\mathsf{T}, \widehat{\mathbf{p}}_n^\mathsf{T}]^\mathsf{T} \in \mathbb{R}^6$ where $\mathbf{p}_n \in \mathbb{R}^3$ and $\widehat{\mathbf{p}}_n \in \mathbb{R}^3$ with $||\widehat{\mathbf{p}}_n|| = 1$ denote the positional and normal vectors respectively, and one target generalised point is defined as $\mathbf{d}_m^q = [\mathbf{q}_m, \widehat{\mathbf{q}}_m]^\mathsf{T} \in \mathbb{R}^6$ where $\mathbf{q}_m \in \mathbb{R}^3$ and $\widehat{\mathbf{q}}_m \in \mathbb{R}^3$ with $||\widehat{\mathbf{q}}_m|| = 1$. We also

define $\mathcal{P} = \{\mathbf{p}_n\}_{n=1}^{N}$ and $\mathcal{Q} = \{\mathbf{q}_m\}_{m=1}^{M}$ for positional vector sets, $\widehat{\mathcal{P}} = \{\widehat{\mathbf{p}}_n\}_{n=1}^{N}$ and $\widehat{\mathcal{Q}} = \{\widehat{\mathbf{q}}_m\}_{m=1}^{M}$ for normal vector sets. For clarity, we further denote the generalised point sets in two spaces as $\mathcal{D}_\mathcal{P} = \{\mathcal{P}, \widehat{\mathcal{P}}\}$ and $\mathcal{D}_\mathcal{Q} = \{\mathcal{Q}, \widehat{\mathcal{Q}}\}$. To simplify the notation, we use the same symbols to denote sets of points and their corresponding matrices, represented as $\mathcal{D}_P \in \mathbb{R}^{N\times 6}$ and $\mathcal{D}_Q \in \mathbb{R}^{M\times 6}$. In order to account for the influence of non-overlapping point pairs in partial-to-full point set registration, we incorporate overlap scores denoted as $\mathbf{o}_p = [o_{p_n}] \in \mathbb{R}^{N\times 1}$ and $\mathbf{o}_q = [o_{q_m}] \in \mathbb{R}^{M\times 1}$into our approach. Given $\mathcal{D}_\mathcal{P}$, $\mathcal{D}_\mathcal{Q}$, $\mathbf{o}_p$ and $\mathbf{o}_q$, the *Generalised Rigid Point Set Registration (GRPSR)* is to estimate the rigid transformation including the rotation matrix $\mathbf{R} \in SO(3)$ and the translation vector $\mathbf{t} \in \mathbb{R}^3$ that best align the two spaces.

IV. HMM-based Point Set Registration with Overlap

A. Hybrid Mixture Models.

The Hybrid Mixture Model (HMM) is a combination of Gaussian Mixture Model (GMM) and Fisher Mixture Model (FMM). It represents the probability distribution over a 6D space as a weighted sum of $J \in N^+$ components, each being a multiplication of Gaussian and Fisher distributions,

$$p(\mathbf{d}_n^p|\mathbf{\Theta}_\mathcal{P}) = \sum_{j=1}^{J} \pi_{p_j} \underbrace{\mathcal{N}(\mathbf{p}_n|\boldsymbol{\mu}_j^p, (\sigma_j^p)^2)}_{\text{Gaussian Distribution}} \underbrace{\mathcal{F}(\widehat{\mathbf{p}}_n|\widehat{\boldsymbol{\mu}}_j^p, \kappa_j^p)}_{\text{Fisher Distribution}}, \quad (1)$$

where $\pi_{p_j} \in [0,1]$ that satisfies $\sum_{j=1}^{J} \pi_{p_j} = 1$ is the mixture weight, $\boldsymbol{\mu}_j^p \in \mathcal{R}^3$ is the mean positional vector and $(\sigma_j^p)^2 \in \mathcal{R}$ is the variance associated with the j-the component, $\widehat{\boldsymbol{\mu}}_j^p \in \mathcal{R}^3(||\widehat{\boldsymbol{\mu}}_j^p|| = 1)$ is the mean normal vector and $\kappa_j \in \mathcal{R}$ is the concentration parameter, and $\mathbf{\Theta}_\mathcal{P} = \{\boldsymbol{\pi}_{p_j}, \boldsymbol{\mu}_j^p, \boldsymbol{\sigma}_j^p, \widehat{\boldsymbol{\mu}}_j^p, \boldsymbol{\kappa}_j^p\}_{j=1}^{J}$. Another probability distribution $p(\mathbf{d}_m^q|\mathbf{\Theta}_\mathcal{Q})$ where $\mathbf{\Theta}_\mathcal{Q} = \{\boldsymbol{\pi}_{q_j}, \boldsymbol{\mu}_j^q, \boldsymbol{\sigma}_j^q, \widehat{\boldsymbol{\mu}}_j^q, \boldsymbol{\kappa}_j^q\}_{j=1}^{J}$ can be similarly defined as that in Eq. (1).

B. HMM-based Point Set Registration with overlap score.

Similar to DeepGMR[6], the registration from $\mathcal{D}_\mathcal{P}$ to $\mathcal{D}_\mathcal{Q}$ can be formulated as a two-step optimization. The fitting step fits HMM $\mathbf{\Theta}_\mathcal{Q}^\star$ to the target generalised point set $\mathcal{D}_\mathcal{Q}$, while the registration step estimates the optimal transformation $\mathbf{T}^\star$ that aligns the source point set $\mathcal{D}_\mathcal{P}$ to $\mathbf{\Theta}_\mathcal{Q}^\star$.

$$\textbf{Fitting: } \mathbf{\Theta}_\mathcal{Q}^\star = \arg\max_{\mathbf{\Theta}_\mathcal{Q}\in\mathcal{H}} p(\mathcal{D}_\mathcal{Q}|\mathbf{\Theta}_\mathcal{Q}), \quad (2)$$

$$\textbf{Registration: } \arg\max_{\mathbf{T}\in \mathrm{SE}(3)} p(\mathbf{T}(\mathcal{D}_\mathcal{P})|\mathbf{\Theta}_\mathcal{Q}^\star), \quad (3)$$

where $\mathrm{SE}(3)$ is the special Euclidean group. $\mathcal{H}$ is the space of permitted HMM parameterisations.

1) Fitting Step: For the fitting step we can employ the EM algorithm to maximize a lower bound on the probability distribution p by introducing a set of latent variables $\mathcal{C}_\mathcal{Q}$, where $\mathcal{C}_\mathcal{Q} = \{c_{mj}^q\}$ with $c_{mj}^q \in [0,1]$ indicating $\mathbf{d}_m^q$ and j-th component of $\mathbf{\Theta}_\mathcal{Q}$.

The EM updates for the fitting step in Eq. (2) are as follows.

$$\mathbf{E}_{\mathbf{\Theta}_\mathcal{Q}} : q(\mathcal{C}_\mathcal{Q}) := p(\mathcal{C}_\mathcal{Q}|\mathcal{D}_\mathcal{Q}, \mathbf{\Theta}_\mathcal{Q}^k), \quad (4)$$

$$\mathbf{M}_{\mathbf{\Theta}_\mathcal{Q}} : \mathbf{\Theta}_\mathcal{Q}^{k+1} := \arg\max_{\mathbf{\Theta}_\mathcal{Q}\in\mathcal{H}} \mathbb{E}_q[\ln p(\mathcal{D}_\mathcal{Q}, \mathcal{C}_\mathcal{Q}|\mathbf{\Theta}_\mathcal{Q})], \quad (5)$$

where $k \in \mathbb{N}^+$ is the number of iterations of EM, $\mathcal{C}_\mathcal{Q} = \{c_{mj}^q\}_{m,j=1,1}^{M,J}$. According to the EM algorithm, the estimation formula of $\mathcal{C}_\mathcal{Q}$ are as follows,

$$\begin{aligned} &p(c_{mj} = 1|\mathbf{d}_m^q, \mathbf{\Theta}_\mathcal{P}^k) \\ &= \frac{p(\mathbf{d}_m^q|c_{mj} = 1, \mathbf{\Theta}_\mathcal{Q}^k)}{\sum_{j=1}^{J} p(\mathbf{d}_m^q|c_{mj} = 1, \mathbf{\Theta}_\mathcal{Q}^k)} \\ &= \frac{\pi_j \mathcal{N}(\mathbf{q}_m|\boldsymbol{\mu}_j^q, (\sigma_j^q)^2)\mathcal{F}(\widehat{\mathbf{q}}_m|\widehat{\boldsymbol{\mu}}_j^q, \kappa_j^q)}{p(\mathbf{d}_m^q|\mathbf{\Theta}_\mathcal{Q}^k)}, \end{aligned} \quad (6)$$

which can be seen as the point-to-distribution posterior correspondence probability between $\mathbf{d}_m^q$ and HMM component center ($\boldsymbol{\mu}_j^q$ and $\widehat{\boldsymbol{\mu}}_j^q$).

Let $\gamma_{mj}^q = \mathbb{E}_q[c_{mj}^q]$, to handle the impact of non-overlapping point pairs in partial-to-full point set registration, we utilise overlap scores $o_q = \{o_{q_m}\}_{m=1}^{M}$ where $o_{q_m} \in [0,1]$ in the HMM parameters. Therefore, the solution for Eq. (5) can be written as

$$\gamma_{mj}^{o_q} = o_{q_m}\gamma_{mj}^q, \ \pi_{q_j}^o = \sum_{m=1}^{M} \gamma_{mj}^{o_q}, \quad (7)$$

$$\boldsymbol{\mu}_j^q = \sum_{m=1}^{M} \frac{\gamma_{mj}^o \mathbf{q}_m}{\pi_{q_j}^o}, \ \widehat{\boldsymbol{\mu}}_j^q = \frac{\sum_{m=1}^{M} \gamma_{mj}^o \widehat{\mathbf{p}}_m}{||\sum_{m=1}^{M} \gamma_{mj}^p o_{q_m} \widehat{\mathbf{q}}_m||}, \quad (8)$$

$$(\sigma_j^q)^2 = \frac{1}{3\pi_{q_j}^o} \sum_{m=1}^{M} (\mathbf{q}_m - \boldsymbol{\mu}_j^q)^\mathsf{T}(\mathbf{q}_m - \boldsymbol{\mu}_j^q), \quad (9)$$

$$r_j = \sum_{m=1}^{M} \frac{\gamma_{mj}^o \widehat{\mathbf{q}}_m^\mathsf{T} \widehat{\boldsymbol{\mu}}_j^q}{\pi_{q_j}^o}, \ \kappa_j = \frac{r_j(3 - r_j^2)}{(1 - r_j^2)}. \quad (10)$$

2) Registration Step: Likewise that in the fitting step, we also adopt the EM to solve the optimization problem of transformation T as follows,

$$\mathbf{E}_\mathbf{T} : q(\mathcal{C}_\mathcal{Q}) := p(\mathcal{C}_\mathcal{Q}|\mathbf{T}^k(\mathcal{D}_\mathcal{P}), \mathbf{\Theta}_\mathcal{Q}^\star), \quad (11)$$

$$\mathbf{M}_\mathbf{T} : \mathbf{T}^{k+1} := \arg\max_{\mathbf{T}\in \mathrm{SE}(3)} \mathbb{E}_q[\ln p(\mathbf{T}(\mathcal{D}_\mathcal{P}), \mathcal{C}_\mathcal{Q}|\mathbf{\Theta}_\mathcal{Q}^\star)]. \quad (12)$$

Considering both the forward and backward processes, the bidirectional HMM-based registration is implemented. In the *forward* process, we are aligning $\mathcal{D}_\mathcal{P}$ using the forward transformation matrix $\mathbf{T}$ with $\mathbf{\Theta}_\mathcal{Q}$. In the *backward* process, we are aligning $\mathcal{D}_\mathcal{Q}$ using the backward transformation matrix $\mathbf{T}^{-1}$ with $\mathbf{\Theta}_\mathcal{P}$. The EM steps that optimize over the transformation parameters $\mathbf{T}$ in the bi-directional manner are as follows.

$$\begin{aligned} \mathbf{E}_\mathbf{T} : q(\mathcal{C}_\mathcal{Q}, \mathcal{C}_\mathcal{P}) :=& p(\mathcal{C}_\mathcal{Q}|\mathbf{T}^k(\mathcal{D}_\mathcal{P}), \mathbf{\Theta}_\mathcal{Q}^\star) \\ &+ p(\mathcal{C}_\mathcal{P}|(\mathbf{T}^k)^{-1}(\mathcal{D}_\mathcal{Q}), \mathbf{\Theta}_\mathcal{P}^\star), \end{aligned} \quad (13)$$

$$\begin{aligned} \mathbf{M}_\mathbf{T} : \mathbf{T}^{k+1} := \arg\max_{\mathbf{T}\in \mathrm{SE}(3)} \mathbb{E}_q[&\ln p(\mathbf{T}(\mathcal{D}_\mathcal{P}), \mathcal{C}_\mathcal{Q}|\mathbf{\Theta}_\mathcal{Q}^\star) + \\ &\ln p(\mathbf{T}^{-1}(\mathcal{D}_\mathcal{Q}), \mathcal{C}_\mathcal{P}|\mathbf{\Theta}_\mathcal{P}^\star)]. \end{aligned} \quad (14)$$

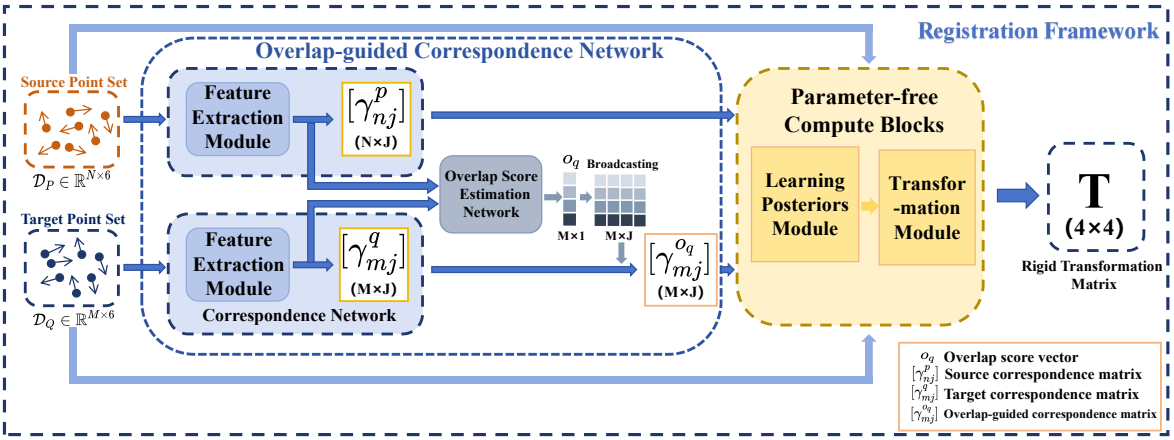

Fig. 2. The overall registration framework of OBHMR. The correspondence network that estimates the correspondence probabilities between generalised points and hybrid mixture models (HMMs) components representing the point set. The overlap estimation network that calculates the overlap score of each point. The learning posterior module that formulates the overlap-guided HMM parameters. Finally, the transformation module that computes the rigid transformation by utilizing the bidirectional registration mechanism, given correspondence and overlap-guided HMM parameters.

V. OBHMR: Bidirectional HMM-based Point Set Registration with Overlap

A. Overlap-guided Correspondence Network

1) Feature Extraction Module: The feature extraction network takes in a generalised point set (e.g., the source generalised point set $\mathcal{D}_\mathcal{P}$) and produces the depth feature for finding correspondence and estimating the overlap region. Inspired by INENET [18], we design a point feature extraction network using Spatial Transformer Network (STN) [19] and PointNet [20], which improves the geometric invariance of features and utilises the normal information.

Firstly, the position vectors and normal vectors are input into the STN to enhance the geometric invariance of the point set. Then, a multi-layer perception (MLP) module with size $(6, 64, 64)$ is utilised to extract deeper-level features, followed by applying the STN once again to enhance the geometric invariance of the output in the feature space. Finally, an MLP$(64, 128, 256, 1024)$ is used to extract the ultimate deep features. So we can obtain two point features matrix $\mathcal{F}_p \in \mathbb{R}^{N\times 1024}$ and $\mathcal{F}_q \in \mathbb{R}^{M\times 1024}$ as,

$$\mathcal{F}_p = f(\Phi(f(\Phi(\mathcal{D}_P)))), \tag{15}$$

$$\mathcal{F}_q = f(\Phi(f(\Phi(\mathcal{D}_Q)))), \tag{16}$$

where $f(\cdot)$ represents MLP layer, $\Phi(\cdot)$ represents STN layer.

2) Correspondence Network: The correspondence network takes in learnt features $\mathcal{F}_q$ of $\mathcal{D}_\mathcal{Q}$ using the FEM, and outputs the correspondence probabilities $\gamma^q_{mj} \in \mathbb{R}$ where $\sum_{j=1}^{J} \gamma^q_{mj} = 1$ for all m. Similarly, using the learnt features $\mathcal{F}_p$ of $\mathcal{D}_\mathcal{P}$ and another correspondence network, the correspondence probabilities $\gamma^p_{nj} \in \mathbb{R}$ are computed where $\sum_{j=1}^{J} \gamma^p_{nj} = 1$ for all n. Each γ^q_{mj} or γ^p_{nj} represents the latent correspondence probability between the $\mathbf{d}^q_m$ or $\mathbf{d}^p_n$ and the j-th component of the corresponding latent HMMs.

3) Overlap Score Estimation Network: After obtaining the point features, we use cosine similarity to calculate the similarity between feature pairs to obtain the feature similarity matrix, which is then processed with MLP$(1024, 512, 128, 1)$ with a sigmoid function to get overlap score $o_{q_m} \in [0, 1]$. The feature similarity matrix between $\mathbf{d}^p_n$ and $\mathbf{d}^q_m$, and the overlap score vector with $\mathcal{D}_\mathcal{Q}$ are formulated as,

$$(M_\mathcal{F})_{mn} = \frac{\mathcal{F}_{q_m}\mathcal{F}^\mathsf{T}_{p_n}}{|\mathcal{F}_{q_m}| \times |\mathcal{F}_{p_n}|}, \tag{17}$$

$$\mathbf{o}_q = MLP_s[M_\mathcal{F}], \tag{18}$$

where $\mathcal{F}_{p_n} \in \mathbb{R}^{1\times 1024}$ and $\mathcal{F}_{q_m} \in \mathbb{R}^{1\times 1024}$ represent the n-th point feature vector in $\mathcal{F}_p$ and the m-th point feature vector in $\mathcal{F}_q$ respectively, MLP_s represents a MLP$(1024, 512, 128, 1)$ together with a sigmoid function, $M_\mathcal{F} \in \mathbb{R}^{M\times N}$ represents the feature similarity matrix, $\mathbf{o}_q \in \mathbb{R}^{M\times 1}$ is the overlap score vector of $\mathcal{D}_\mathcal{Q}$. Since the target point set $\mathcal{D}_P$ is the partial subset of the source point set $\mathcal{D}_Q$, all points in $\mathcal{D}_P$ are assumed in the overlap region and $\mathbf{o}_p \in \mathbb{R}^{N\times 1}$ is defined as a vector with all elements 1 (i.e., $o_{p_n} = 1$).

B. Parameter Calculation Module

With the simplified assumptions that all mixture components share the common weights, all positional variance and concentration parameters are the same across the data points $\mathcal{D}_\mathcal{Q}$, summarised as $\pi^q_j = \frac{1}{J_q}$, for $j = 1, ..., J_q$, $(\sigma^q_1)^2 = ...(\sigma^q_j)^2... = (\sigma^q_{J_q})^2 = \sigma^2$, and $\kappa^q_1 = ...\kappa^q_j... = \kappa^q_{J_q} = \kappa$. Taking $\mathcal{D}_\mathcal{Q}$ as an example, the estimation of the mean positional/normal vectors $\boldsymbol{\mu}^q_j$ and $\widehat{\boldsymbol{\mu}}^q_j$ are similar to those in Eq. (8) while the other two parameters σ^2 and κ in $\boldsymbol{\Theta}_\mathcal{Q}$ are estimated with

$$\sigma^2 = \frac{\sum_{j=1}^{J}\sum_{m=1}^{M} \gamma^{o_q}_{mj}(\mathbf{q}_m - \boldsymbol{\mu}^q_j)^\mathsf{T}(\mathbf{q}_m - \boldsymbol{\mu}^q_j)}{3\sum_{j=1}^{J} \pi^o_{q_j}}, \tag{19}$$

$$\kappa = \frac{\sum_{j=1}^{J}\sum_{m=1}^{M} \gamma^{o_q}_{mj}\widehat{\mathbf{q}}^\mathsf{T}_m\widehat{\boldsymbol{\mu}}^q_j}{\sum_{j=1}^{J} \pi^o_{q_j}}. \tag{20}$$

C. Bi-directional Transformation Module

The Bi-directional Transformation Module is given as follows. At the beginning, the maximum likelihood objective is to minimize the sum of KL-divergence between the transformed latent source distribution $\mathsf{T}(\mathbf{\Theta}_{\mathcal{P}})$ and latent target distribution $\mathbf{\Theta}_{\mathcal{Q}}$ (i.e., forward), between the transformed latent target distribution $\mathsf{T}^{-1}(\mathbf{\Theta}_{\mathcal{Q}})$ and latent source distribution $\mathbf{\Theta}_{\mathcal{P}}$ (i.e., backward) as:

$$\mathsf{T}^{\star} = \arg\min_{\mathsf{T}} \underbrace{\mathrm{KL}(\mathsf{T}(\mathbf{\Theta}_{\mathcal{P}})|\mathbf{\Theta}_{\mathcal{Q}})}_{\text{forward}} + \underbrace{\mathrm{KL}(\mathsf{T}^{-1}(\mathbf{\Theta}_{\mathcal{Q}})|\mathbf{\Theta}_{\mathcal{P}})}_{\text{backward}}, \tag{21}$$

where the forward transformation operation $\mathsf{T}(\bullet)$ with rotation $\mathbf{R}$ and $\mathbf{t}$ is $\mathsf{T}(\mathbf{p}_n) = \mathbf{R}\mathbf{p}_n + \mathbf{t}$ and $\mathsf{T}(\widehat{\mathbf{p}}_n) = \mathbf{R}\widehat{\mathbf{p}}_n$ with which $\mathsf{T}(\boldsymbol{\mu}_j^p)$ and $\mathsf{T}(\widehat{\boldsymbol{\mu}}_j^p)$ can computed similarly. On the other hand, the operation of the inverse transformation matrix $\mathsf{T}^{-1}(\bullet)$ with the corresponding rotation $\mathbf{R}^{\mathsf{T}}$ and translation $-\mathbf{R}^{\mathsf{T}}\mathbf{t}$ is defined as $\mathsf{T}^{-1}(\mathbf{q}_m) = \mathbf{R}^{\mathsf{T}}\mathbf{q}_m - \mathbf{R}^{\mathsf{T}}\mathbf{t}$ and $\mathsf{T}^{-1}(\widehat{\mathbf{q}}_m) = \mathbf{R}^{\mathsf{T}}\widehat{\mathbf{q}}_m$ with which $\mathsf{T}^{-1}(\boldsymbol{\mu}_j^q)$ and $\mathsf{T}^{-1}(\widehat{\boldsymbol{\mu}}_j^q)$ can be computed in the similar manner. After manipulations that are similar to those in [6], the *forward* and *backward* objective functions $\mathcal{L}_{\text{forward}}$ and $\mathcal{L}_{\text{backward}}$ to be minimized are respectively

$$\mathcal{L}_{\text{forward}} = \sum_{n,j=1}^{N,J} \gamma_{nj}^{o_p}\Big(\frac{1}{2\sigma^2}||\mathsf{T}(\mathbf{p}_m) - \boldsymbol{\mu}_j^q||^2 - \kappa(\mathbf{R}\widehat{\mathbf{p}}_n)^{\mathsf{T}}\widehat{\boldsymbol{\mu}}_j^q\Big), \tag{22}$$

and $\mathcal{L}_{\text{backward}}$ is:

$$= \sum_{m,j=1}^{M,J} \gamma_{mj}^{o_q}\Big(\frac{1}{2\sigma^2}||\mathsf{T}^{-1}(\mathbf{q}_m) - \boldsymbol{\mu}_j^p||_2^2 - \kappa(\mathbf{R}^{\mathsf{T}}\widehat{\mathbf{q}}_m)^{\mathsf{T}}\widehat{\boldsymbol{\mu}}_j^p\Big), \tag{23}$$

where from the first to the second line we have adopted the distance-preserving property of the rigid transformation. Then the overall objective function is:

$$\mathcal{L}_{\text{bidirectional}} = \mathcal{L}_{\text{forward}} + \mathcal{L}_{\text{backward}}. \tag{24}$$

Translation Vector. In the bi-directional HMM-based registration scenario, the optimal translation $\mathbf{t}^{\star}$ is computed by solving $\frac{\partial \mathcal{L}_{\text{bidirectional}}}{\partial \mathbf{t}} = \mathbf{0}$ which results in

$$\mathbf{t}^{\star} = \boldsymbol{\mu}_{V_p}^{\text{bidirectional}} - \mathbf{R}\boldsymbol{\mu}_q^{\text{bidirectional}} \tag{25}$$

where $\boldsymbol{\mu}_p^{\text{bidirectional}}$ and $\boldsymbol{\mu}_q^{\text{bidirectional}}$ are

$$\begin{aligned}\boldsymbol{\mu}_q^{\text{bi}} &= \frac{\sum_{n,j=1}^{N,J}\gamma_{nj}^{o_p}\boldsymbol{\mu}_j^q + \sum_{m,j=1}^{M,J}\gamma_{mj}^{o_q}\mathbf{q}_m}{\sum_{n,j=1}^{N,J}\gamma_{nj}^{o_p} + \sum_{m,j=1}^{M,J}\gamma_{mj}^{o_q}},\\ \boldsymbol{\mu}_p^{\text{bi}} &= \frac{\sum_{n,j=1}^{N,J}\gamma_{nj}^{o_p}\mathbf{p}_n + \sum_{m,j=1}^{M,J}\gamma_{mj}^{o_q}\boldsymbol{\mu}_j^p}{\sum_{n,j=1}^{N,J}\gamma_{nj}^{o_p} + \sum_{m,j=1}^{M,J}\gamma_{mj}^{o_q}}.\end{aligned} \tag{26}$$

The Rotation Matrix. The objective function related with $\mathbf{R}^{\star}$, after substituting Eq. (25) into Eq. (24), can be simplified as

$$\mathbf{R}^{\star} = \arg\max_{\mathbf{R}} \mathrm{Tr}\Big(\mathbf{R}\mathbf{H}\Big), \tag{27}$$

where $\mathbf{H}$ is defined as

$$\begin{aligned}\mathbf{H} = \frac{1}{\sigma^2}\sum_{j=1}^{J}\Big(\sum_{n=1}^{N}\gamma_{nj}^{o_p}\mathbf{p}_n'(\boldsymbol{\mu}_j^{q'})^{\mathsf{T}} + \sum_{m=1}^{M}\gamma_{mj}^{o_q}\boldsymbol{\mu}_j^{p'}(\mathbf{q}_m')^{\mathsf{T}}\Big)\\ + \kappa\sum_{j=1}^{J}\Big(\sum_{n=1}^{N}\gamma_{nj}^{o_p}\widehat{\mathbf{p}}_n(\widehat{\boldsymbol{\mu}}_j^q)^{\mathsf{T}} + \sum_{m=1}^{M}\gamma_{mj}^{o_q}\widehat{\boldsymbol{\mu}}_j^p(\widehat{\mathbf{q}}_m)^{\mathsf{T}}\Big)\end{aligned} \tag{28}$$

where $\mathbf{q}_m' = \mathbf{q}_m - \boldsymbol{\mu}_q^{\text{bi}}$, $\boldsymbol{\mu}_j^{p'} = \boldsymbol{\mu}_j^p - \boldsymbol{\mu}_{V_p}^{\text{bi}}$ and $\boldsymbol{\mu}_j^{q'} = \boldsymbol{\mu}_j^q - \boldsymbol{\mu}_q^{\text{bi}}$, $\mathbf{p}_n' = \mathbf{p}_n - \boldsymbol{\mu}_{V_p}^{\text{bi}}$.

By conducting the singular value decomposition (SVD) of $\mathbf{H}$ as $\mathbf{H} = \mathbf{U}\mathbf{S}\mathbf{V}^{\mathsf{T}}$, we can get the updated rotation matrix $\mathbf{R}^{\star}$ as

$$\mathbf{R}^{\star} = \mathbf{V}\mathrm{diag}([1, 1, \det(\mathbf{V}\mathbf{U}^{\mathsf{T}})])\mathbf{U}^{\mathsf{T}}. \tag{29}$$

D. Loss function

Since correspondence network and overlap score estimation network need to be considered by loss function, the training loss is the sum of two loss functions, i.e., $\mathcal{L}_{\text{train}} = \mathcal{L}_{\text{overlap}} + \mathcal{L}_{\text{Reg}}$.

1) Overlap Score Loss: Since the goal of the overlap score loss is to detect the overlap region between $\mathcal{D}_{\mathcal{Q}}$ and $\mathcal{D}_{\mathcal{P}}$, we can use the binary cross entropy loss. The ground-truth overlap lable $\mathbf{M}_g^m$ is first computed as,

$$\mathbf{M}_g^m = \begin{cases}1 & \text{if } \mathbf{q}_m \text{ lies in the overlap region,}\\ 0 & \text{otherwise.}\end{cases} \tag{30}$$

Therefore, the overlap score loss function is defined as:

$$\mathcal{L}_{\text{overlap}} = \sum_{m=1}^{M}\mathbf{M}_g^m\log\mathbf{o}_{\mathbf{q}_m} + (1-\mathbf{M}_g^m)\log(1-\mathbf{o}_{\mathbf{q}_m}). \tag{31}$$

2) Global Registration Loss: Given the ground-truth transformation matrix $\mathbf{T}_{\text{gt}}$ that transforms $\mathcal{D}_{\mathcal{P}}$ to $\mathcal{D}_{\mathcal{Q}}$, the mean-squared error is minimized as

$$\mathcal{L}_{\text{Reg}} = ||\mathbf{T}\mathbf{T}_{\text{gt}}^{-1} - \mathbf{I}||^2 + ||\mathbf{T}_{\text{gt}}\mathbf{T}^{-1} - \mathbf{I}||^2 \tag{32}$$

where $\mathbf{T}$ is the 4×4 transformation matrix that contains the rotation matrix and translation vector, $\mathbf{I} \in \mathbb{R}^{4\times 4}$ is the identity matrix.

VI. Experimental Results

In computer-assisted orthopedic surgery, the image-to-patient registration that aligns the pre-operative full model and intra-operative partial data is a challenging partial-to-full registration task essentially. To demonstrate the superiority of OBHMR in this scenario, we evaluate OBHMR against conventional methods including ICP [10], CPD [8], BCPD[9], deep-learning-based methods including FMR [11], PointNetLK++ [12], hybrid registration methods including DeepGMR [6], UGMM [7], and the partial registration methods including Predator [13], RegTR [14], OGMM [17] on the human femur and hip models in MedShapeNet [21].

Evaluation Metrics. We use the rotation error

TABLE I

QUANTITATIVE RESULTS ON PARTIAL POINT SETS OF HUMAN HIP MODELS.

Method	Overlap Ratio 50%				Overlap Ratio 70%			
	Rot (°)	Trans (mm)	RMSE (mm)	P-value	Rot (°)	Trans (mm)	RMSE (mm)	P-value
ICP[10]	23.83 ± 12.57	25.00 ± 0.00	43.20 ± 20.28	3.12×10^{-92}	21.22 ± 13.47	24.89 ± 0.00	40.33 ± 18.22	5.11×10^{-110}
CPD[8]	21.72 ± 18.17	46.49 ± 24.33	47.24 ± 24.36	3.22×10^{-76}	10.19 ± 5.62	22.36 ± 12.57	23.00 ± 12.38	1.75×10^{-72}
BCPD[9]	25.50 ± 23.05	24.68± 6.05	44.91 ± 28.13	1.26×10^{-65}	21.76 ± 13.08	24.03 ± 3.26	37.54 ± 18.57	4.71×10^{-99}
FMR[11]	22.93 ± 17.49	34.54 ± 19.68	35.30 ± 20.04	6.84×10^{-54}	8.84 ± 5.75	15.31 ± 8.60	16.03 ± 8.61	1.75×10^{-72}
PointNetLK++[12]	24.96 ± 14.96	43.20 ± 15.26	46.30 ± 12.93	1.27×10^{-99}	12.34 ± 8.07	19.75 ± 10.00	20.83 ± 9.83	7.60×10^{-90}
DeepGMR[6]	11.08 ± 6.36	17.99 ± 9.74	20.84 ± 10.20	3.14×10^{-74}	6.11 ± 4.38	11.18 ± 5.70	12.54 ± 6.22	2.01×10^{-68}
UGMM[7]	26.56 ± 16.54	23.46 ± 11.92	34.61 ± 16.47	1.39×10^{-95}	36.08 ± 32.57	26.81 ± 20.31	39.23 ± 31.36	7.82×10^{-59}
Predator[13]	10.11 ± 8.97	12.33 ± 11.37	13.22 ± 11.07	6.17×10^{-117}	7.31 ± 5.88	9.22 ± 7.51	11.41 ± 10.31	9.07×10^{-137}
RegTR[14]	6.32 ± 5.91	9.22 ± 8.31	15.49 ± 13.26	7.32×10^{-05}	3.87 ± 3.03	4.69 ± 4.24	8.64 ± 7.73	3.67×10^{-07}
OGMM[17]	6.71 ± 6.67	7.23 ± 6.72	19.83 ± 20.01	2.07×10^{-09}	4.32 ± 4.10	4.79 ± 4.48	13.63 ± 12.99	1.89×10^{-13}
BHMR(*Ours*)	5.32 ± 2.83	14.57 ± 6.74	13.18 ± 5.82	5.82×10^{-32}	3.51 ± 1.91	9.45 ± 4.18	9.36 ± 3.70	7.94×10^{-48}
OBHMR(*Ours*)	**3.17 ± 2.27**	**4.94 ± 3.36**	**5.41 ± 3.86**	-	**1.65 ± 1.03**	**2.68 ± 1.85**	**2.89 ± 1.52**	-

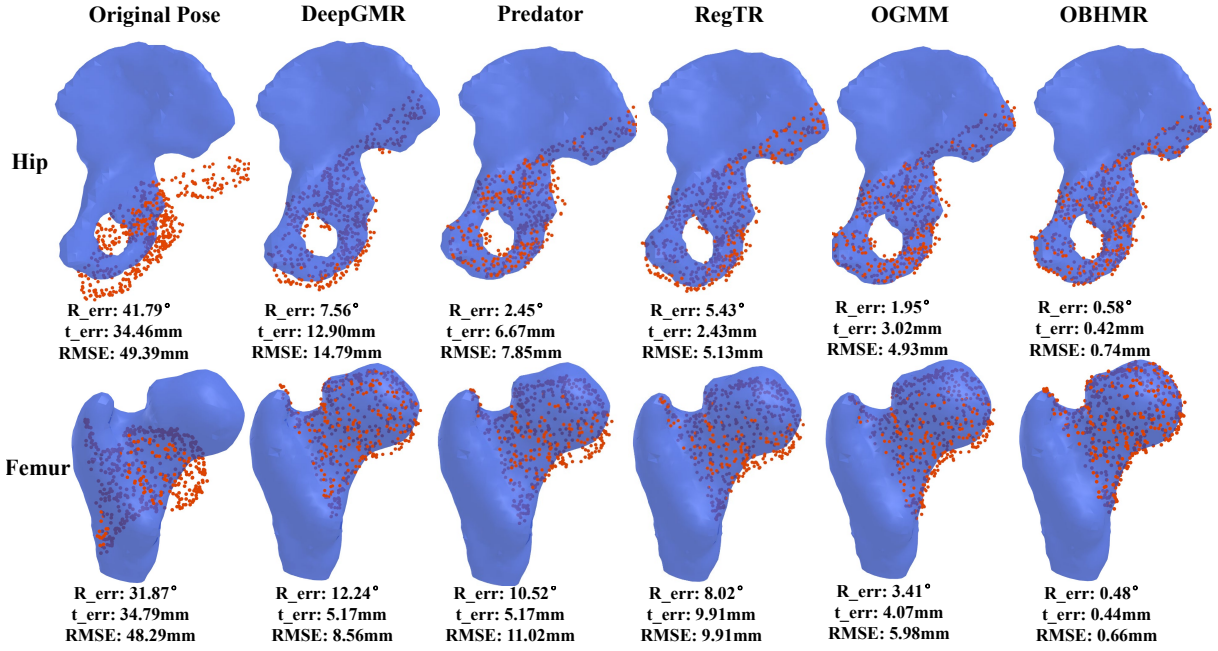

Fig. 3. Qualitative results of partial-to-full registrations with a 50% overlap ratio on noisy hip (cf. the first row) and femur (cf. the second row) models. The preoperative full mesh and partial intraoperative points are shown in blue and red respectively. Each column depicts the registration performance with a specific method, while the first column denotes the case before registration. The registration error values of each example are labeled below each sub-plot.

$\text{Error}_{\text{Rot}} = \arccos\left[\frac{\text{tr}(\mathbf{R}_{\text{true}}\mathbf{R}_{\text{cal}}^{\top})-1}{2}\right] \times \frac{180^{\circ}}{\pi}$ and the translation error $\text{Error}_{\text{Trans}} = \|\mathbf{t}_{\text{cal}} - \mathbf{t}_{\text{true}}\|_2$ to evaluate registration accuracy, which are measured in degree and milimeter respectively. Following DeepGMR [6], we also assess the average RMSE. Finally, to verify the statistical significance of the experimental results, we conduct paired-tests using the RMSE results and present p-values between OBHMR and compared methods at $\alpha = 0.01$ significance level.

Datasets. The MedShapeNet dataset [21] contains more than $100,000$ medical shape models including femur, hip, skull, and lung, etc. In this study, We utilise 1301 hip and 1457 femur models in MedShapeNet. For the femur dataset, we sample 1024 points from femur model and normalize each point set within an unit box $[0, 1]^3$. During the training process, the rigid rotation matrix is randomly sampled in the range $[0, 45]^{\circ}$ with arbitrarily chosen axes and translation in the range $[0, 50]$ mm. For the hip dataset, we followed the similar approach.

Implementation Details. In the correspondence network introduced in Sect. V-A, PointNet with STN is first utilised as the backbone to extract high-dimensional features from the generalised point sets. Taking $\mathcal{D}_{\mathcal{P}}$ as an example, the global high-dimensional features are concatenated with point-wise local features, together with softmax, the point-to-distribution correspondence can be estimated. The number of HMM components J is 16. The Adam optimizer is used for training the network for 300 epochs with the batch size being 32. The initial learning rate is set to 0.001. If the validation loss fails to improve for more than 10 epochs, the learning rate is halved. All learning-based registration methods are implemented in Pytorch and trained on one NVIDIA GeForce RTX 4090 GPU.

TABLE II

QUANTITATIVE RESULTS ON PARTIAL POINT SETS OF HUMAN FEMUR MODELS.

Method	Overlap Ratio 50%				Overlap Ratio 70%			
	Rot (°)	Trans (mm)	RMSE (mm)	P-value	Rot (°)	Trans (mm)	RMSE (mm)	P-value
ICP[10]	21.61 ± 15.15	26.72 ± 20.70	25.08 ± 19.11	1.78×10^{-100}	21.15 ± 12.80	25.00 ± 0.00	36.05 ± 18.43	3.92×10^{-121}
CPD[8]	21.13 ± 16.98	26.79 ± 17.85	24.28 ± 16.79	9.83×10^{-44}	20.14 ± 12.92	26.99 ± 20.35	24.32 ± 19.44	5.51×10^{-54}
BCPD[9]	24.95 ± 16.86	24.16 ± 3.86	39.50 ± 25.89	1.22×10^{-70}	22.36 ± 14.00	24.66 ± 4.37	37.32 ± 21.22	6.01×10^{-91}
FMR[11]	30.09 ± 25.42	27.11 ± 23.17	27.51 ± 23.26	3.44×10^{-44}	11.96 ± 10.04	12.72 ± 13.81	13.27 ± 14.27	1.91×10^{-64}
PointNetLK++[12]	38.04 ± 25.51	34.23 ± 27.36	34.75 ± 26.72	2.69×10^{-50}	12.34 ± 8.07	19.75 ± 10.00	20.83 ± 9.83	3.84×10^{-37}
DeepGMR[6]	12.44 ± 9.29	19.96 ± 12.90	21.92 ± 14.78	1.05×10^{-59}	7.53 ± 5.13	13.24 ± 11.71	14.54 ± 13.16	2.48×10^{-43}
UGMM[7]	51.87 ± 38.23	35.97 ± 24.01	37.93 ± 30.15	1.55×10^{-59}	45.61 ± 31.80	34.21 ± 20.91	33.46 ± 25.89	1.68×10^{-67}
Predator[13]	12.73 ± 10.61	15.13 ± 13.71	16.87 ± 14.58	5.50×10^{-134}	8.71 ± 11.27	11.27 ± 9.37	13.22 ± 12.14	6.70×10^{-159}
RegTR[14]	6.98 ± 6.09	8.73 ± 7.41	12.05 ± 11.65	4.70×10^{-07}	3.97 ± 3.21	4.79 ± 4.17	7.69 ± 6.30	7.78×10^{-13}
OGMM[17]	5.07 ± 4.87	6.85 ± 6.87	16.63 ± 16.04	3.21×10^{-09}	3.43 ± 3.30	4.06 ± 3.97	8.29 ± 7.93	5.59×10^{-09}
BHMR(*Ours*)	6.32 ± 4.39	9.59 ± 7.20	8.49 ± 6.22	8.59×10^{-19}	3.73 ± 3.02	4.04 ± 3.83	4.01 ± 3.32	7.43×10^{-08}
OBHMR(*Ours*)	**5.36 ± 4.03**	**5.62 ± 4.20**	**4.88 ± 3.04**	-	**2.67 ± 2.21**	**3.19 ± 2.69**	**2.91 ± 2.32**	-

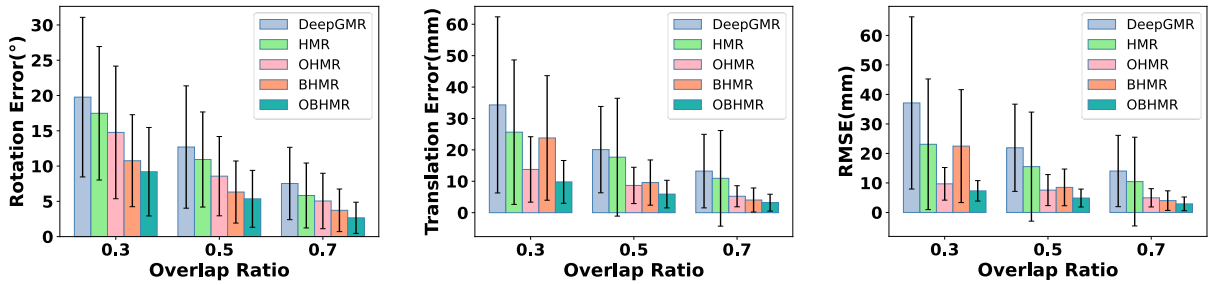

Fig. 4. The three error bar plots represent the mean and standard deviation values of the rotation error (left), translation error (middle), and RMSE (right) at different overlap ratios in ablation studies(cf. Sect. VI-C), which evaluates the effectiveness of individual components.

A. Evaluation on Partial and Noisy hip dataset

We set two different overlap ratios (i.e., 70%, 50%) to evaluate OBHMR against compared approaches. To increase the experiment's resemblance to real-world scenarios, each pair of point sets was subject to isotropic Gaussian noise, with the magnitude of noise varying between 0 mm and 3.81 mm. During the test process, the range of rigid transformation is same as those in training. Note that 1041 hip models are used to train, while 260 hip models are used for validation and test.

Table I shows the quantitative results for the hip dataset with an overlap ratio of 70% and 50%, which shows that OBHMR outperforms all other compared methods. All p-values of the paired t-tests obtained using results of OBHMR and compared methods were smaller than 0.01 (cf. Table I), indicating the significant improvements. Note that we denote our proposed method where the overlap score estimation module in Sect. V-A.3 is removed as BHMR. The performance of OBHMR is significantly better ($p < 0.001$) than BHMR (no less than 40% improvement in all metrics) thanks to the overlap score estimation network. Fig. 3 shows the corresponding qualitative results.

B. Evaluation on Partial and Noisy Femur dataset

This sub-experiment evaluates OBHMR against other methods on the human femur bone. The overlap ratio's setting and the range of rigid transformation and injected Gaussion noise in two point sets are the same as those in Sect. VI-A. Note that 1166 femur models are used to train, while 291 femur models are used for validation and test.

Table. II shows the quantitative results on femur dataset with an overlap ratio of 70% and 50%, for all compared methods. Fig. 3 shows the qualitative results. Similar observations with those in Sect. VI-A can be found, i.e., the proposed OBHMR approach significantly outperforms both compared methods and BHMR ($p < 0.001$).

C. Ablation Study

Ablation studies are conducted on the femur dataset using 30%, 50%, and 70% overlap ratios to evaluate the effectiveness of different components in OBHMR, where other experimental settings are the same as Sect. VI-B. We denote our method where the bi-directional mechanism in Sect. V-C is removed as OHMR, where both overlap score prediction and bi-directional mechanism are removed as HMR. And the proposed registration network without normal vectors, is actually DeepGMR [6].

Fig. 4 shows the corresponding quantitative results. Again, we compute p-values of paired t-tests between different methods to assess the statistical significance of differences or improvements. The observations can be summarised as: (1) the improved performance of HMR compared to DeepGMR (p-value = $7.73 \times 10^{-22} < 0.001$) validates the effectiveness of the utilised additional normal information. (2) the better performance of BHMR compared to HMR (p-value = $1.58 \times 10^{-4} < 0.01$) demonstrates the benefit of leveraging the bi-directional mechanism. (3) By comparing

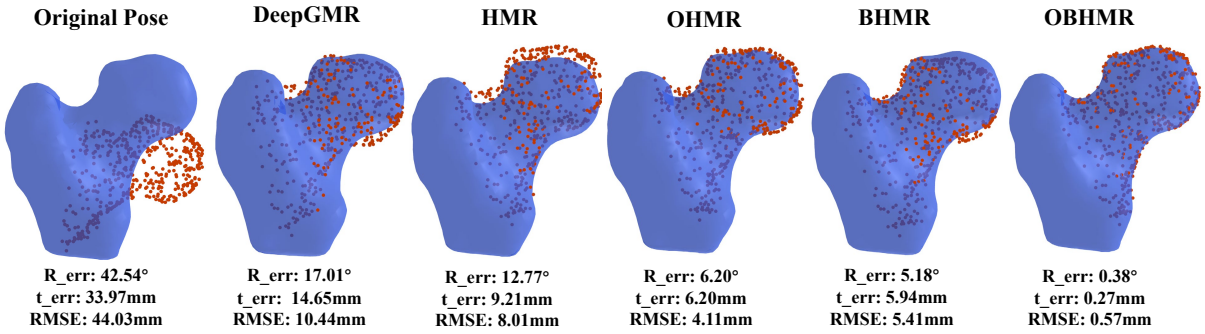

Fig. 5. The qualitative results of different methods under a 50% overlap ratio, where the preoperative full mesh and partial intraoperative points are shown in blue and red respectively. The registration error values of each example are labeled below each sub-plot.

OHMR with HMR (p-value = $6.34 \times 10^{-12} < 0.001$), and OBHMR with BHMR (p-value = $2.17 \times 10^{-10} < 0.001$), the significance of the overlap score estimation module is validated. Fig. 5 shows qualitative results under the 50% overlap ratio, which verifies the findings.

VII. CONCLUSIONS

This paper proposes OBHMR, a novel and accurate learning-based generalized point set registration approach for computer-assisted orthopedic surgery, where normal vectors and an additional overlap score estimation module are utilised while a bidirectional registration mechanism is leveraged to consider noise in both point sets. Extensive results on the human bone dataset across a range of overlap ratios demonstrate the remarkable registration accuracy and great capability to deal with partial-to-full registration problems. The effectiveness of each module, i.e., the overlap estimation module, the incorporated additional geometric information and the bidirectional registration mechanism, has been confirmed through ablation studies. In the future, we will explore deeper geometric features to address the registration problem with lower overlap ratios.

REFERENCES

[1] C. Li, L. Wang, C. Perka, and A. Trampuz, "Clinical application of robotic orthopedic surgery: a bibliometric study," *BMC musculoskeletal disorders*, vol. 22, pp. 1–14, 2021.

[2] Z. Min, A. Zhang, Z. Zhang, J. Wang, S. Song, H. Ren, and M. Q.-H. Meng, "3d rigid point set registration for computer-assisted orthopedic surgery (caos): A review from the algorithmic perspective," *IEEE Transactions on Medical Robotics and Bionics*, 2023.

[3] R. H. Taylor, N. Simaan, A. Menciassi, and G.-Z. Yang, "Surgical robotics and computer-integrated interventional medicine," *Proceedings of the IEEE*, vol. 110, no. 7, pp. 823–834, 2022.

[4] A. Zhang, Z. Min, L. Liu, and M. Q.-H. Meng, "Generalized 3-d rigid point set registration with bidirectional hybrid mixture models," *IEEE Transactions on Automation Science and Engineering*, pp. 1–12, 2023.

[5] Z. Zhang, A. Zhang, J. Lai, H. Ren, R. Song, Y. Li, M. Q.-H. Meng, and Z. Min, "Ghmm: Learning generative hybrid mixture models for generalized point set registration in computer-assisted orthopedic surgery," *IEEE Transactions on Medical Robotics and Bionics*, vol. 6, no. 3, pp. 1285–1295, 2024.

[6] W. Yuan, B. Eckart, K. Kim, V. Jampani, D. Fox, and J. Kautz, "Deepgmr: Learning latent gaussian mixture models for registration," in *Computer Vision–ECCV 2020: 16th European Conference, Glasgow, UK, August 23–28, 2020, Proceedings, Part V 16*. Springer, 2020, pp. 733–750.

[7] X. Huang, S. Li, Y. Zuo, Y. Fang, J. Zhang, and X. Zhao, "Unsupervised point cloud registration by learning unified gaussian mixture models," *IEEE Robotics and Automation Letters*, vol. 7, no. 3, pp. 7028–7035, 2022.

[8] A. Myronenko and X. Song, "Point set registration: Coherent point drift," *IEEE transactions on pattern analysis and machine intelligence*, vol. 32, no. 12, pp. 2262–2275, 2010.

[9] O. Hirose, "A bayesian formulation of coherent point drift," *IEEE transactions on pattern analysis and machine intelligence*, vol. 43, no. 7, pp. 2269–2286, 2020.

[10] P. J. Besl and N. D. McKay, "Method for registration of 3-d shapes," in *Sensor fusion IV: control paradigms and data structures*, vol. 1611. Spie, 1992, pp. 586–606.

[11] X. Huang, G. Mei, and J. Zhang, "Feature-metric registration: A fast semi-supervised approach for robust point cloud registration without correspondences," in *Proceedings of the IEEE/CVF conference on computer vision and pattern recognition*, 2020, pp. 11 366–11 374.

[12] X. Li, J. K. Pontes, and S. Lucey, "Pointnetlk revisited," in *Proceedings of the IEEE/CVF conference on computer vision and pattern recognition*, 2021, pp. 12 763–12 772.

[13] S. Huang, Z. Gojcic, M. Usvyatsov, A. Wieser, and K. Schindler, "Predator: Registration of 3d point clouds with low overlap," in *Proceedings of the IEEE/CVF Conference on computer vision and pattern recognition*, 2021, pp. 4267–4276.

[14] Z. J. Yew and G. H. Lee, "Regtr: End-to-end point cloud correspondences with transformers," in *Proceedings of the IEEE/CVF conference on computer vision and pattern recognition*, 2022, pp. 6677–6686.

[15] H. Thomas, C. R. Qi, J.-E. Deschaud, B. Marcotegui, F. Goulette, and L. J. Guibas, "Kpconv: Flexible and deformable convolution for point clouds," in *Proceedings of the IEEE/CVF international conference on computer vision*, 2019, pp. 6411–6420.

[16] S. Umeyama, "Least-squares estimation of transformation parameters between two point patterns," *IEEE Transactions on Pattern Analysis & Machine Intelligence*, vol. 13, no. 04, pp. 376–380, 1991.

[17] G. Mei, F. Poiesi, C. Saltori, J. Zhang, E. Ricci, and N. Sebe, "Overlap-guided gaussian mixture models for point cloud registration," in *Proceedings of the IEEE/CVF Winter Conference on Applications of Computer Vision*, 2023, pp. 4511–4520.

[18] Y. Wu, Y. Zhang, X. Fan, M. Gong, Q. Miao, and W. Ma, "Inenet: Inliers estimation network with similarity learning for partial overlapping registration," *IEEE Transactions on Circuits and Systems for Video Technology*, vol. 33, no. 3, pp. 1413–1426, 2023.

[19] M. Jaderberg, K. Simonyan, A. Zisserman, and k. kavukcuoglu, "Spatial transformer networks," in *Advances in Neural Information Processing Systems*, C. Cortes, N. Lawrence, D. Lee, M. Sugiyama, and R. Garnett, Eds., vol. 28. Curran Associates, Inc., 2015.

[20] C. R. Qi, H. Su, K. Mo, and L. J. Guibas, "Pointnet: Deep learning on point sets for 3d classification and segmentation," in *Proceedings of the IEEE conference on computer vision and pattern recognition*, 2017, pp. 652–660.

[21] J. Li, A. Pepe, C. Gsaxner, G. Luijten, Y. Jin, N. Ambigapathy, E. Nasca, N. Solak, G. M. Melito, A. R. Memon *et al.*, "Medshapenet–a large-scale dataset of 3d medical shapes for computer vision," *arXiv preprint arXiv:2308.16139*, 2023.